Model-Based Imaging of Cardiac Apparent Conductivity and Local Conduction Velocity for Diagnosis and Planning of Therapy

Phani Chinchapatnam*, Kawal S. Rhode, Matthew Ginks, C. Aldo Rinaldi, Pier Lambiase, Reza Razavi, Simon Arridge, and Maxime Sermesant

***Abstract*—We present an adaptive algorithm which uses a fast electrophysiological (EP) model to estimate apparent electrical conductivity and local conduction velocity from non-contact mapping of the endocardial surface potential. Development of such functional imaging revealing hidden parameters of the heart can be instrumental for improved diagnosis and planning of therapy for cardiac arrhythmia and heart failure, for example during procedures such as radio-frequency ablation and cardiac resynchronisation therapy. The proposed model is validated on synthetic data and applied to clinical data derived using hybrid X-ray/magnetic resonance imaging. We demonstrate a qualitative match between the estimated conductivity parameter and pathology locations in the human left ventricle. We also present a proof of concept for an electrophysiological model which utilises the estimated apparent conductivity parameter to simulate the effect of pacing different ventricular sites. This approach opens up possibilities to directly integrate modelling in the cardiac EP laboratory.**

***Index Terms*—Electrophysiology, cardiac conductivity imaging, conduction velocity, parameter estimation, eikonal models**

I. Introduction

The human heart is stimulated by electrical impulses to facilitate coordinated contraction of the cardiac chambers. Any irregularities in the heart rhythm are referred to as *arrhythmia*. Cardiac arrhythmia is a cause of considerable morbidity and mortality in addition to constituting a huge cost burden to modern health-care systems. Although arrhythmia can be controlled by pharmacological treatment, curative procedures are increasingly being undertaken in the form of radio-frequency ablation (RFA). Prior to ablation, an essential invasive diagnostic procedure is performed (the electrophysiological study (EPS)) in which the arrhythmia circuit is mapped within the cardiac chambers. EPS involves placing electrodes within the heart in specific locations to determine the nature of the arrhythmia and its source within the heart. This information allows the cardiologist to diagnose the problem as well as determine the appropriate treatment. However, the identification of arrhythmia propagation (ectopic foci, accessory pathways and areas of slow conduction) by analysing the measured electrical data often requires expert intervention and can be highly complex. The measured electrical data is obtained either in the form of endocardial potentials at discrete points, or as isochrones of depolarisation and repolarisation on reconstructed endocardial/epicardial surfaces. Another rapidly evolving field is cardiac resynchronisation therapy (CRT) for treatment of heart failure. This involves correction of uncoordinated contractile function of the heart, which itself results from delayed electrical activation. This pathological process occurs frequently in patients with heart failure. By implanting a pacemaker device using three electrical leads, the activation of the heart can be resynchronised, resulting in more efficient pump function, thereby improving both symptoms and prognosis [1]. A further clinical application of electrophysiology is the reversal of life-threatening heart rhythm disturbance (ventricular arrhythmia) by defibrillation, which uses a short burst of high energy to restore the heart's normal rhythm. Implantable devices also have the capability to deliver the energy required to achieve this. For all these clinical applications, augmentation of measured isochronal data with additional maps related to electrical conduction parameters of the myocardial tissue may be highly beneficial in the management of cardiac arrhythmia.

Cardiac imaging modalities such as magnetic resonance imaging (MRI) and computed tomography (CT) can provide accurate anatomical and functional information and substantial research is being devoted to integrating the anatomical information derived from these modalities with electrical mapping to guide procedures such as RFA and CRT [2]. Hybrid X-ray/magnetic resonance (XMR) suites are a new type of clinical facility combining an MR scanner and a cardiac X-ray system that share a common patient table. Registration of the two image spaces (MR and X-ray) makes it possible to combine patient anatomy with electrophysiologic data [3].

Manuscript received January 08, 2008; revised May 15, 2008. This work was supported in part by the UK-EPSRC under grant EP/D060877/1, the UK-DTI technology programme grant 17352 and Philips Healthcare, Best, the Netherlands. *Asterisk indicates corresponding author*.

Phani Chinchapatnam (email: p.chinchapatnam@cs.ucl.ac.uk) and Simon Arridge are with the Centre for Medical Image Computing, University College London, Gower Street, London, WC1E 6BT, U.K.

Kawal S. Rhode, Matthew Ginks and Reza Razavi are with the Interdisciplinary Medical Imaging Group, Division of Imaging Sciences, King's College London, 4th Floor Lambeth Wing, St Thomas' Hospital, London, SE1 7EH, U.K.

C. Aldo Rinaldi is with the Department of Cardiology, Guy's and St Thomas' NHS Foundation Trust, St Thomas' Hospital, London, SE1 7EH, U.K.

Pier Lambiase is with the Heart Hospital, University College London Hospitals NHS Foundation Trust, London, NW1 2PG, U.K.

Maxime Sermesant is with the Asclepios project, INRIA, Sophia-Antipolis, France and the Interdisciplinary Medical Imaging Group, Division of Imaging Sciences, King's College London, 4th Floor Lambeth Wing, St Thomas' Hospital, London, SE1 7EH, U.K.

Copyright (c) 2008 IEEE. Personal use of this material is permitted. However, permission to use this material for any other purposes must be obtained from the IEEE by sending a request to pubs-permissions@ieee.org.

Although these procedures can be highly effective with minimal side effects, they still have suboptimal success rates in some groups of patients. There is still a need for substantial innovation in guiding these interventions, both in streamlining the procedures themselves and in improving patient outcomes.

The use of electrophysiologic models simulating electrical propagation for various cardiac arrhythmias will facilitate and improve the efficacy of these interventional procedures. Existing models however are computationally expensive and are presently not suitable for direct use in the cardiac catherisation laboratory. The aim of our research is to design electrophysiological models that are suited for clinical use, and to evaluate methods to combine these models with interventional data. More specifically in this paper, we present a method to image conduction parameters, which is intended to provide more detailed assessment of cardiac electrophysiological function in order to aid in the guidance of interventional procedures.

Modelling the entire electrophysiology of the heart begins with the incorporation of electrical phenomena from the microscopic cellular level into the macroscopic field using a set of partial differential equations (PDEs) modelling a continuum. A wide variety of models simulating the electrical activity of the heart have been developed from accurate cellular models such as Luo and Rudy models [4], [5] to phenomenological models [6]–[9] and eikonal models [10], [11]. Although, Luo and Rudy models and phenomenological models provide sufficiently accurate resolution of the electrical (depolarisation and repolarisation) phenomena, they are computationally demanding due to a very small spatial scale associated with the electrical propagation in comparison to the size of the ventricles. Fortunately, as the depolarisation occurs only in a narrow region, the depolarisation region can be considered as a propagating wavefront [11] and an eikonal equation can be derived describing this activation phenomenon. The motion of the activation wavefront is observed on a larger spatial scale thus resulting in much faster computations. Furthermore, the solution of these models cannot be directly correlated with pathologies due to the complex interaction of various parameters present in the models. We believe that development of algorithms for identifying the hidden parameters in electrophysiological models would help cardiologists in diagnosis and treatment of pathologies. For our interventional purpose and as parameter adjustment often requires several simulations, we propose to use the eikonal equation to model the electrophysiology. We hope that by using the eikonal model at least certain types of conduction abnormalities such as left bundle branch block could be simulated with sufficient accuracy and hence can be useful in a clinical setting. The most common method of solving the electrical propagation PDEs numerically is by the finite element method (FEM) which incurs a considerable amount of computational cost. We propose a different solution technique based on the fast marching method (FMM) [12] which comes under the category of single-pass methods. FMM exploits the causality of the solution variable and hence solves the equation on a mesh of N vertices with $\mathcal{O}(N \log(N))$ complexity, thus tending towards satisfying clinical time constraints.

In this paper, we use a novel FMM for the numerical solution of the anisotropic eikonal-diffusion (ED) equation on surface triangulations and propose an adaptive zonal decomposition iterative algorithm to estimate an apparent conductivity parameter. The definition of the apparent conductivity parameter and its relation to the intrinsic myocardial tissue specific conductivity is detailed later in the paper. This parameter is estimated first on a global basis and then local corrections are made. The developed model is validated on synthetic data and then applied to clinical data. We show that the proposed estimation procedure can potentially aid in the detection of scarred/infarcted regions in the myocardium using electrophysiological and geometrical information and also in the prediction of the electrical propagation for different pacing conditions.

II. Electrophysiology Model

Cardiac tissue is highly anisotropic with wave speeds that differ substantially depending on their direction. For example, in human myocardium, longitudinal propagation is about 0.5 m/s along the fibres and about 0.17 m/s transverse to the fibres. In this section, we present a fast electrophysiological model of depolarisation wavefront propagation on anisotropic cardiac surfaces.

The state of the art of modelling electrical activity in ventricular cells can be classified into biophysical cellular models (i.e., Luo-Rudy) and phenomenological cellular models (i.e., FitzHugh-Nagumo). Biophysical models use ion concentrations as state variables and solve for the different currents through the membrane. In contrast, phenomenological models directly use the resulting transmembrane potential (or extra and intra cellular potentials) as state variable. Both these type of cellular models can be introduced into a spatial diffusion framework (which may be either mono-domain or bi-domain) for simulating electrical propagation on ventricles (i.e., more than one cell). Due to fast dynamics of depolarisation, the solution of these equations is computationally demanding and hence quite intractable in a clinical setting. Ignoring the effects of repolarisation, eikonal models can be built to simulate the propagation of the depolarisation wave in quiescent tissue. These eikonal models are given by the eikonal-curvature (EC) [10] and the eikonal-diffusion (ED) equation [13]. Tomlinson et al. [11] have analysed these two equations and found that the ED equation is nearer to the actual propagation than the EC equation. The EC equation requires a critical amount of depolarised tissue to sustain the depolarisation wave propagation while the ED equation does not place any such constraint. In view of this reason, we chose to solve the ED equation in our model.

The static ED equation for the depolarisation time ($T(\mathbf{x})$) in the myocardium is given by

$$c_0 \sqrt{D(\mathbf{x})} \left(\sqrt{\nabla T(\mathbf{x})^t \mathbf{M} \nabla T(\mathbf{x})} \right) - \nabla \cdot (D(\mathbf{x}) \mathbf{M} \nabla T(\mathbf{x})) = \tau(\mathbf{x}), \tag{1}$$

where the superscript t denotes transpose, c_0 is a dimensionless constant related to the cell membrane and $\tau(\mathbf{x})$ is the cell membrane time constant. $D(\mathbf{x})$ is the square of the tissue space constant along the fibre and is related to the specific conductivity of the tissue. The tensor quantity relating to the

fibre directions is given by $\mathbf{M} = \mathbf{A}\bar{\mathbf{D}}\mathbf{A}^t$, where $\mathbf{A}$ is the matrix defining the fibre directions in the global coordinate system and $\bar{\mathbf{D}} = \mathrm{diag}(1, \lambda^2, \lambda^2)$. λ is the anisotropic ratio of space constants transverse and along the fibre direction and is of the order 0.4 in human myocardium [11].

The nonlinear Equation (1) is solved using a fixed point iterative method combined with a very fast eikonal solver based on a modified anisotropic FMM [14], [15]. The FMM is a single-pass algorithm to solve the classical eikonal equation (without the diffusion term $\nabla \cdot (D\mathbf{M}\nabla T)$) and an anisotropic version was developed earlier as part of this project. At each fixed point iteration, computation of the diffusion term was carried out using P1 Lagrange finite elements. Experimental evidence suggests no flux on the myocardial surface, so we use Neumann boundary condition. We integrate this in the stiffness matrix $K : K_{ij} = \int \nabla\phi_i \ \mathbf{M}\nabla\phi_j$ coming from an integration by parts of the diffusion term in the variational form with ϕ_i and ϕ_j the P1 Lagrange shape functions. The complete details are presented in Algorithm 1.

Algorithm 1 Algorithm for eikonal-diffusion equation

- Inputs: Geometry, site of earliest activation, D
- Solve Eq. (1) without diffusion term using modified FMM [15] to get an initial estimate T_0. Set $T_{\mathrm{curr}} = T_0$.

while convergence achieved != *true* **do**

- Compute anisotropic diffusion flow term $\nabla \cdot (D\mathbf{M}\nabla T)$ with the current estimate T_{curr}.
- Solve for T_{new} using modified FMM [15] $c_0\sqrt{D}\left(\sqrt{\nabla T_{\mathrm{new}}^t \mathbf{M}\nabla T_{\mathrm{new}}}\right) = \tau + \nabla \cdot (D\mathbf{M}\nabla T_{\mathrm{curr}})$

if $\|T_{\mathrm{new}} - T_{\mathrm{curr}}\| < \varepsilon$ **then**

- convergence achieved=true

else

- $T_{\mathrm{curr}} = T_{\mathrm{new}}$

end if

end while

As the method is based on fast marching which is an $\mathcal{O}(N \log(N))$ algorithm, where N denotes the number of points in the mesh, the electrical propagation is solved at a much faster rate as compared to the bi-domain or mono-domain equation based models. For example, the solution of a 5000 node mesh can be achieved in the order of a few seconds [16], and hence the method is suitable for faster computations required in real-time interventional cases.

III. Apparent Conductivity Parameter Estimation

When using electro-anatomic mapping (EAM), cardiologists generally base their analysis of electrophysiological data on the isochrones of depolarisation and repolarisation of the endocardium. However, these time variables may be difficult to interpret due to the influence of the geometry and curvature of the propagating wavefront. The estimation of additional parameter maps related to myocardial tissue property could be beneficial for cardiologists in more rapid interpretation of the data. To realise this goal we have not resorted to a pure signal processing approach, where for instance conduction velocity could be estimated from distance between two isochronal curves [17]. Instead, we propose to estimate the conductivity parameters in the electrophysiology model described in the previous section by posing an inverse problem [18], [19]. The diffusion coefficient D is the square of the effective space constant along the fibre direction and thus an intrinsic property of the myocardial tissue. $D = \lambda_f^2 = \sigma_f \bar{r}_m$, where λ_f is the space constant along the fibre direction, σ_f is the inverse of the sum of effective resistivities of intra and extra cellular domains and $\bar{r}_m$ is the inverse of membrane conductance per unit area. From the above relation and as we model the electrical propagation on a surface (2D), we now refer to the diffusion coefficient D as apparent conductivity (AC) in the rest of the paper. The AC value provides an indication of the region of influence of the excitation wavefront at a particular point [20]. Further, the apparent propagation velocity of the electrical wave in the tissue can also be estimated by $v_{\mathrm{app}} = c_0\sqrt{D}/\tau$ (m/s). In this section, we present an algorithm to estimate the apparent conductivity by matching the isochrones of depolarisation simulated using the EP model to those obtained from clinical measurements. Furthermore, we have an additional advantage in that the model, after parameter estimation, can also be used in a predictive fashion.

The present state of the art in obtaining in vivo electrophysiological assessment are the electro-anatomical mapping systems (Ensite, Carto). Ensite [21] is a non-contact mapping system which utilises a multi-electrode array inserted into the cardiac chamber of interest, and electrical recordings are displayed on an anatomical surface of the endocardium which may be imported from prior imaging or reconstructed using a roving catheter steered endocardially to create the chamber geometry. The Carto system [22] is a contact mapping system where the position of the catheter is obtained using a magnetic tracking system and the electrical recordings are obtained from the tip of the contact catheter. Using these systems the electrical wave propagation can be identified on the endocardial surface. Any isochrones of depolarisation obtained from such mapping systems can be utilised as the measurement data for the estimation procedure. As we have only one measure which is the depolarisation time, we propose to estimate the apparent conductivity D in this paper. The dimensionless constant c_0 is set at 2.5 and the cell time constant τ is set at 1.0 ms respectively. The AC estimation algorithm is divided into two stages namely global and local.

A. Global Conductivity

A nominal value of the AC D_{global} is first sought which minimises the mean error between the measured and simulated isochrones of depolarisation. This global estimation step enables us to bring the simulated isochrones using the model to the scale of measured isochrones and also provides us with a good initial estimate of AC for the local parameter estimation. The global estimation is done using a bisection method and is detailed in Algorithm 2.

B. Local Conductivity

Once the simulated depolarisation time map globally fits the measured one, a local adjustment of the model is possible.

Algorithm 2 Algorithm for Estimating Global Conductivity

- Set $D_{\text{curr}} = D_u$, where D_u is the given user estimate for conductivity parameter.
- Evaluate the average value of measured depolarisation time $\overline{T^m}$

while convergence achieved != *true* **do**
- Solve Eq. (1) using FMM algorithm in Section II with $D = D_{\text{curr}}$ and calculate the average of simulated depolarisation time $\overline{T^s}$.

if $|\overline{T^s} - \overline{T^m}| < \varepsilon$ **then**
- $D_{\text{global}} = D_{\text{curr}}$

convergence achieved = *true*

else

if $\overline{T^s} < \overline{T^m}$ **then**
- $D_{\text{curr}} = D_{\text{curr}} - 0.5 D_{\text{curr}}$

else
- $D_{\text{curr}} = D_{\text{curr}} + 0.5 D_{\text{curr}}$

end if

end if

end while

Gradient based minimisation techniques are generally used for parameter estimation inverse problems. However, in our case as the gradient calculation often tends to be expensive without a suitable adjoint approach, we propose a specific estimation algorithm suited to our fast electrophysiology model.

As the local conductivity estimation falls in the purview of parameter estimation techniques, we resort to the zonal decomposition of the conductivity parameter. We begin by dividing the 2d-surface Ω into M equal zones $R = \{\Omega_1, \Omega_2, \cdots, \Omega_M\}$. The conductivity is then assumed to be given by

$$D(\mathbf{x}) = \sum_{j=1}^{M} D_j \phi_j(\mathbf{x}), \tag{2}$$

where the basis function on the j^{th} zone is given by

$$\phi_j(\mathbf{x}) = \begin{cases} 1 & \mathbf{x} \in \Omega_j \\ 0 & \mathbf{x} \notin \Omega_j \end{cases}.$$

Thus the dimension of the problem is reduced to M. The apparent conductivity values are obtained by minimising the discrete cost function given by

$$\mathcal{C}(\mathbf{D}) = \frac{1}{\mathcal{N}(\nu)} \sum_{v \in \nu} [T_v^m - T_v^s(D_{\Omega_1}, D_{\Omega_2}, \cdots, D_{\Omega_M})]^2, \tag{3}$$

where ν denotes the set of all the vertices of the surface mesh and $\mathcal{N}(.)$ denotes the set's cardinality, T_v^m denotes the measured depolarisation time at the vertex v and $T_v^s(D_{\Omega_1}, D_{\Omega_2}, \cdots, D_{\Omega_M})$ denotes the depolarisation time obtained by solving the fast electrophysiological model with the apparent conductivity values set as $\{D_{\Omega_j}\}_{j=1}^{M}$.

We propose a multilevel approach to the estimation problem. We begin with a minimum number of sub-divisions (zones) of the surface. At each level, an iterative approach is used to estimate the zonal conductivity values. At each iteration we estimate a conductivity value for each region. To further reduce the computational burden on the parameter estimation, we propose to solve the minimisation problem by varying the AC value on one considered region and keeping all other region's AC constant. Thus, the M-dimensional problem is converted into a sequence of K one dimensional minimisation problems. It is to be noted that the order in which the zones are considered is important if one undertakes such a methodology due to the causality of the electrical wave propagation on the surface [19]. Hence the zone set R is pre-ordered according to the mean measured depolarisation times of all the vertices present in that zone i.e.,

$$\bar{T}^m_{\Omega_k} < \bar{T}^m_{\Omega_{k+1}} \quad \forall k = 1, 2, \cdots, M-1.$$

The most popular way of minimising the cost functional is based on the computation of the derivative of the cost function with respect to the parameter. However, in our case as obtaining the derivative involves computing $\partial T / \partial D$ which can only be obtained using finite differences, we resort to a one-dimensional minimisation strategy like the Brent's method [23]. The Brent's minimisation algorithm is utilised to estimate the apparent conductivity value for each zone sequentially. The Brent's method requires an initial bracketing of the minimum and then the minimum is reached by fitting a parabola in the bracketed region. The iterations at a particular level are continued until the difference in the cost function values between two successive iterations falls below a certain threshold ($\varepsilon = 0.01$). Then we proceed to the next level by subdividing the zone with the maximum value of the regional cost function (see Fig.1), defined as

$$\mathcal{C}_{\Omega_j} = \frac{1}{N_j} \sum_{\mathbf{x} \in \Omega_j} [T^m(\mathbf{x}) - T^s(\mathbf{x})]^2.$$

where N_j denotes the number of vertices in the zone Ω_j At the next level, the conductivity values are again estimated on each zone sequentially in the order of the zonal measured depolarisation time according to the iterative Brent method explained earlier. The complete procedure is summarised in the Algorithm 3.

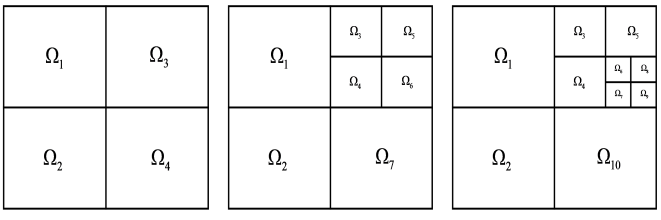

(a) Initial (b) Level I (c) Level II

Fig. 1. (a) Initial zonal decomposition (b) Level 1 zonal decomposition (c) Level 2 decomposition At each level, the zone with maximal $\mathcal{C}_{\Omega_j}$ in the previous level is divided into 4 equal regions.

It is well known that for solving inverse problems, some sort of regularisation is always needed to obtain a meaningful estimate of the parameter. In the presented algorithm, we smooth the AC value at each vertex by taking an area-weighted average of the apparent conductivity of each triangle surrounding the considered vertex. This smoothing enables to improve the convergence of the iterative procedure and also aids in regularisation.

Algorithm 3 Adaptive zonal algorithm for estimating local apparent conductivity

- Construct an initial decomposition of the surface mesh into 4 zones in the order of measured depolarisation times ($R = \{\Omega_1, \cdots, \Omega_4\}$)

while !(convergence achieved or maximum subdivisions reached) **do**
  converged at level=false
  while converged at level != *true* **do**
    for $i = 1$ to $i = \mathcal{N}(R)$ **do**
      - Solve for the zonal AC value using the Brent's minimisation

    end for
    if $|C_i - C_{i-1}| < \varepsilon$ **then**
      - converged at level = *true*

    end if
  end while
  - Find the region with the maximum $\mathcal{C}_{\Omega_j}$ and subdivide
  - Re-order the zones according to measured depolarisation time

end while

It is to be noted that the subdivision of zones is limited by the mesh resolution and at any iteration, if the maximal $\mathcal{C}_{\Omega_j}$ region cannot be further subdivided, we proceed to subdivide the region with the next maximum value. So, the maximum number of zones into which the mesh can be divided is the total number of points in the mesh. However, we stop our iterations if the number of zones at any level reaches a predefined limit set to 64.

IV. Validation of Results

A. AC estimation algorithm

The performance of the adaptive AC parameter estimation algorithm is evaluated initially on simulated data. The electrical data is simulated on a surface mesh of the endocardium consisting of 256 vertices and 480 triangles. A low conductivity region with apparent conductivity $D = 0.1$ was defined on the lateral side of the endocardial mesh and on the remaining points, the AC was set to 0.64 (Fig.2a). The low conductivity region is considered as diseased tissue and the regions with $D = 0.64$ are considered healthy. The depolarisation time presented in Fig.2b and Fig.2c is the result of a simulation based on the EP model for $c_0 = 2.5$, $\lambda = 0.4$ and $\tau = 1$ ms with this conductivity map.

The apparent conductivity estimation algorithm presented in section III is tested on this synthetic data initially. To start the estimation, a crude estimate for AC was taken as $D_u = 2.0$ on the whole surface. The global estimation algorithm predicted a mean value of $D_{\text{global}} = 0.58$ and the mean error between the measured and simulated depolarisation times dropped from 4.02 ms to 2.8 ms. We also examined the robustness of the global estimation procedure by using different initial values ranging from $D_u = 0.1$ to $D_u = 2.0$ (see Fig.3a). From the figure, it can be seen that the proposed global estimation algorithm is quite robust to user initial guess.

We now proceed to use this value (D_{global}) as the initial guess of AC for the adaptive zonal conductivity estimation algorithm. The entire surface was initially divided into 4 equal regions. The Brent's optimisation routine requires an initial bracketing of the minimum. In this paper, we use $[0.01, \bar{D}, 10.0]$ as the bracketing where $\bar{D}$ is the apparent conductivity value estimated at the previous iteration for that particular region. After stopping of the algorithm, we obtain a total of 64 subdivisions of the endocardial surface. The convergence of the root mean squared (r.m.s) error between measured and simulated depolarisation times across iterations is shown in Fig.3b. We see that the error drops rapidly until the number of zones are around 16 to 20 and afterwards the convergence tends to become slow. So, if one desires a quick estimate, the algorithm could be stopped after the number of zones become around 20. We obtain a final r.m.s error of 1.42 ms and a mean error of 0.84 ms for depolarisation times ranging from 0 to 96 ms. The absolute error between measured and depolarisation times before and after the adaptive zonal estimation algorithm procedure is shown in Fig.4b and Fig.4c respectively. Fig.4a shows the estimated apparent conductivity map on the surface after convergence. Comparing Fig.4a and Fig.2a, it can be clearly seen that the presented algorithm is able to identify regions of low conductivity.

The AC estimation algorithm is now tested for its robustness to cardiac fibre directions. A Gaussian noise of zero mean with a standard deviation of 10^o [1] was added [24], and the resultant AC images estimated by the algorithm are examined (See Fig.5). We obtain a similar result to the case when there was no noise in the fibre directions thus proving that the presented algorithm is also robust to noise or uncertainty in cardiac fibre directions.

Further, to evaluate the effect of mesh resolution on the apparent conductivity estimation algorithm, we subdivided each triangle in the 256 node mesh into four triangles by joining the midpoints of each triangle edge and ran the estimation algorithm with the measured data resolution fixed at the original 256 points. Results obtained on synthetic data show that the estimation algorithm is able to identify regions of low conductivity for both the coarse as well as fine mesh with similar resolution (see Fig.6).

V. Clinical data

In this section, we present the results of the adaptive conduction parameter imaging algorithm on clinical data. We evaluate the performance on data acquired from patients with a Left Bundle Branch Block (LBBB) pathology. In brief, the left branch of the bundle of His-Purkinje system of these patients is damaged and hence the initialisation of left ventricular activation derives mainly from the septal region instead of an apical site via the Purkinje network. The patients underwent EPS where an Ensite array is inserted into the left ventricle via a retrograde aortic approach. A locator signal from a standard steerable ablation catheter is utilised to construct left ventricular chamber geometry. The Ensite array comprises

[1] A 10^o variability was chosen as a probable value of the normal variability of fibre orientations, based on a study conducted by Peyrat et al. [24].

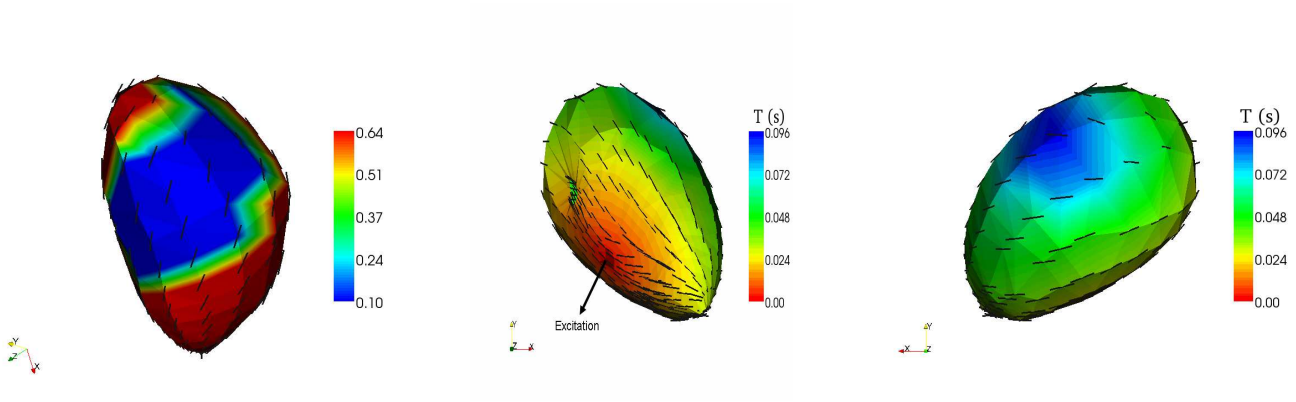

(a) Simulated AC (b) Isochrones (View 1) (c) Isochrones (View 2)

Fig. 2. (a) AC map used to generate synthetic data. The blue region represents area of low conductivity (diseased) as compared to the healthy region represented in red. (b),(c) Resultant isochrones of depolarisation (sec) obtained using the fast EP model.The excitation begins in the septal region and ends in the lateral region. The black lines on the mesh indicate the fibre directions pre-set to $+60^o$ to the circumferential direction.

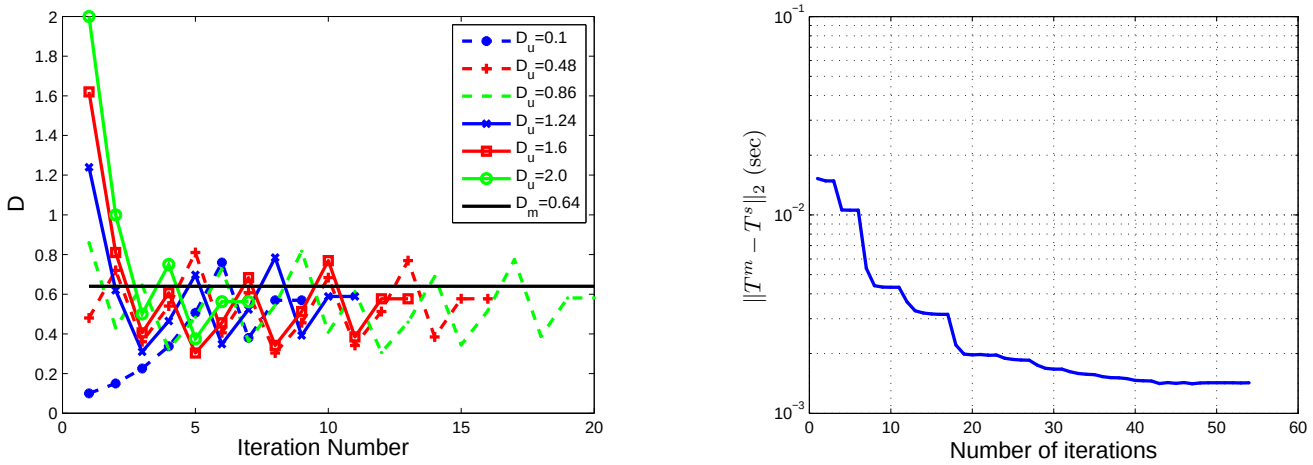

(a) Global estimation (b) Local estimation

Fig. 3. Convergence graphs for global estimation procedure (a) and local estimation algorithm (b). In (a), the horizontal black line indicates the value of $D = 0.64$ which was the nominal value of AC on healthy tissue used to generate measured data.

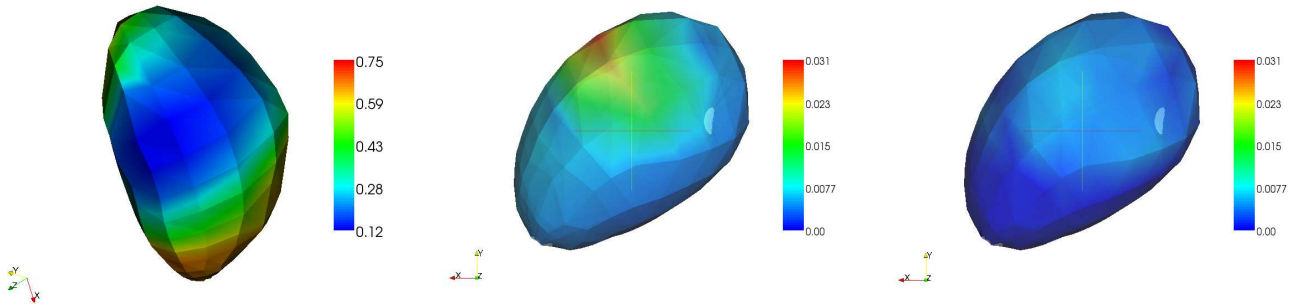

(a) Estimated AC (b) Absolute Error (Initial) (c) Absolute Error (After)

Fig. 4. (a) Estimated AC colour map after convergence of zonal adaptive estimation algorithm. (b),(c) Absolute Error between measured and estimated depolarisation times (sec) before and after zonal adaptive estimation respectively.

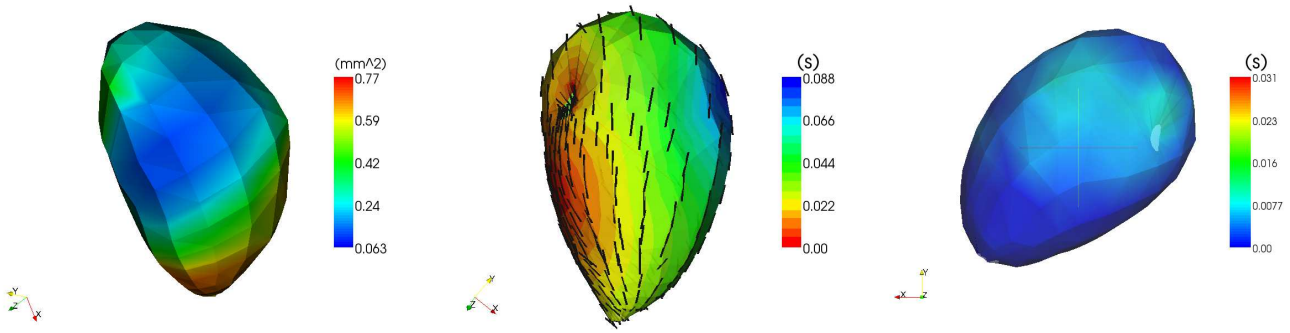

(a) Estimated AC (b) Isochrones (model) (c) Absolute Error (After)

Fig. 5. Results obtained from the AC estimation procedure using fibre directions corrupted with a Gaussian noise with a mean of 0^o and a standard deviation of 10^o (a) Estimated AC image (b) Isochrones of depolarisation obtained after the AC estimation procedure and (c) Absolute error between measured and simulated depolarisation times.

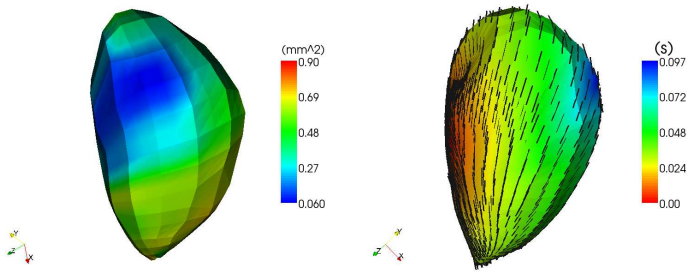

(a) Estimated AC (b) Isochrones (model)

Fig. 6. Effect of mesh resolution on AC parameter estimation algorithm (a) Estimated AC map (b) Isochrones of depolarisation predicted by the EP model with estimated conductivity map.

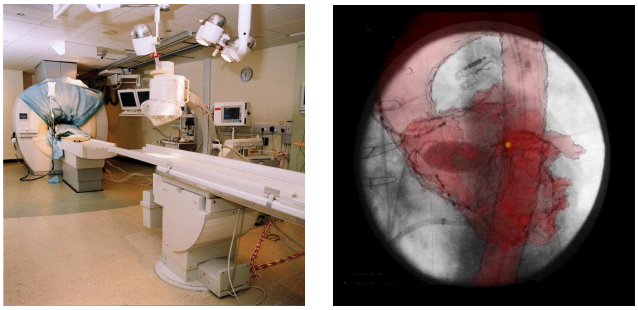

(a) XMR Room (b) XMR Registration

Fig. 7. (a) XMR suite at Guy's Hospital, London. (Front) X-ray C-arm system, (Back) MR scanner (b) Registration of X-ray and MR images using optical tracking methodology [3]. The 3D volume (transparent red) obtained from MR is overlaid on to the X-ray image.

a 9 F multi electrode array (MEA) mapping catheter and local endocardial potentials are reconstructed employing the inverse solution method [25]. The data was acquired in an XMR environment (see Fig.7). The patient was imaged using MRI prior to the EPS to obtain a 3D Steady-State Free-Precession (SSFP) image of the heart (typical parameters for imaging are 256×256 matrix, 200 slices, resolution = $1.05 \times 1.05 \times 7.2\text{mm}^3$, TR=$14.0$ ms, TE=6.05 ms, flip angle=15^o, scan time $\approx$ 6 min). The Ensite reconstructed chamber can then be registered to the endocardial surface obtained from MR using an earlier developed and validated registration technique based on optical tracking [3], [26].

Fig.8a shows the isochrones of depolarisation reconstructed on 256 points as measured by the Ensite system for one such EP case. The initialisation (initial activation of the left ventricle) begins at the septal region and ends in the lateral region of the ventricle. The standard values for the constants that we use in the model are $c_0 = 2.5$, $\lambda = 0.4$ and $\tau = 1.0$ ms. We apply the AC estimation algorithm (Section III) for this case and the resultant isochrones of depolarisation and the apparent conductivity image estimated by the model are shown in Fig.8b and Fig.8c respectively. The black lines in Fig.8b represent the fibre directions (60^o to circumferential direction). We obtain a final r.m.s error between the measured and simulated depolarisation times of 16 ms from an initial error of 62 ms. The reconstructed endocardial surface was divided into 55 zones at convergence.

In order to validate the estimated AC map for this case, we endeavour to compare the predicted regions of low apparent conductivity to the regions of scar obtained from segmentation of a late enhancement MR image performed by a clinician who was blinded to all electrophysiological data. Initially, the reconstructed surface of the left ventricular chamber from Ensite is deformed to fit the ventricle surface obtained from MR image. The deformed Ensite surface registered with the MR image [28] is shown in Fig.9a. Fig.9b and Fig.9c show the estimated AC map and the segmented scars in the same coordinate system. The dark blue regions on the deformed mesh identify regions on the mesh with a low AC, which we believe correlate to regions of slow conduction. From these figures, it can be seen that the areas of slow conduction and scars were co-localised to the accuracy of the MRI to Ensite registration. It is to be noted that as the late enhancement images were acquired one day before the procedure, the

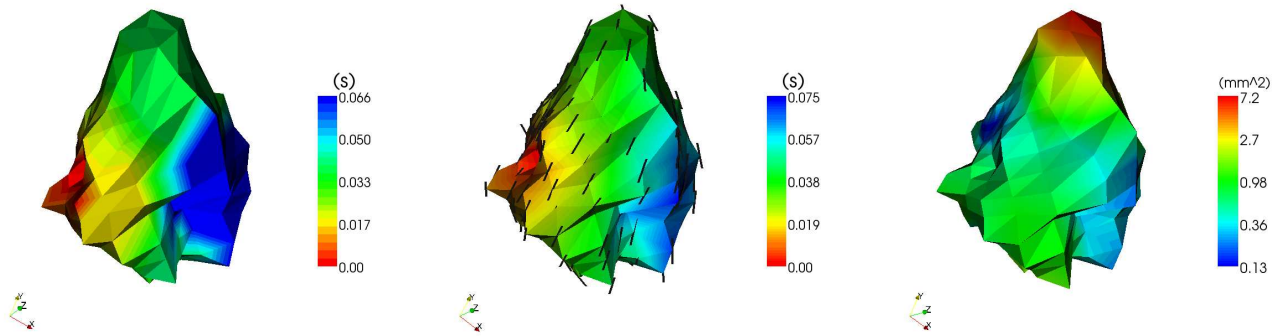

(a) Isochrones (Ensite) (b) Isochrones (model) (c) Estimated AC

Fig. 8. (a) Isochrones of depolarisation obtained from Ensite (b) Isochrones of depolarisation obtained from EP model after estimating apparent conductivity (c) Estimated AC colour map after convergence.

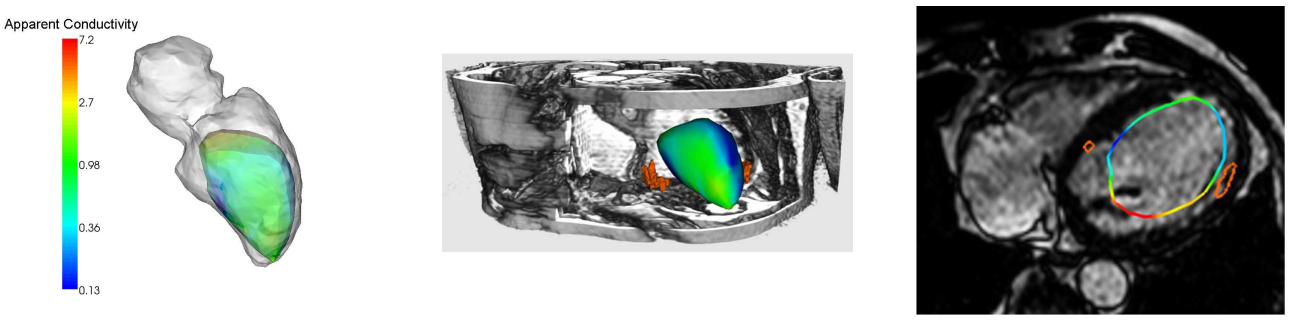

(a) Ensite to MR registration (b) Scar comparison (c) Scar comparison

Fig. 9. (a) Registration of Ensite endocardial anatomy to MR derived anatomy (transparent white), the colourmap on the Ensite anatomy represents the estimated apparent conductivity; (b),(c) Comparison of scar locations (orange) obtained from segmentation of the late enhancement MR image to areas of low apparent conductivity on the deformed Ensite anatomy in volume rendered SSFP MR image and a 2D axial slice respectively (Images obtained using Cardioviz3D [27]).The colourmap values on the Ensite anatomy (b) and Ensite contour (c) are the same as in (a).

sources of error are the registration of pre-operative late enhancement images to the 3D MR images acquired on the day of procedure and also the registration between the Ensite and MR derived surfaces. Furthermore, as indicated in earlier section III, additional parameter maps of apparent conduction velocity $v_{\text{app}} = c_0\sqrt{D}/\tau$ can also be generated after estimating AC. The apparent conduction velocity images for this case are detailed in Fig.10. The apparent conduction velocity for normal tissue regions is around 2.5 m/s and in regions of scar, the conduction velocity drops to approximately 0.9 m/s.

We now present results for a second case of LBBB pathology. Fig.11a shows the measured depolarisation time isochrones for the baseline mode (normal sinus rhythm). The application of the presented algorithm resulted in the model predicting the depolarisation isochronal map as shown in Fig.11b. The r.m.s error between measured and estimated depolarisation times was 27 ms after the estimation as compared to 113 ms before the estimation procedure. Next, the registration of the Ensite reconstructed ventricular surface with that of MR surface is shown in Fig.11c. The colour map on the Ensite surface shows the estimated apparent conductivity and the black surface to the septal side indicates the scar location obtained from late enhancement image segmentation. It can clearly be seen that the top part of the Ensite reconstructed ventricle is in the aortic root and hence the results obtained from the Ensite system in that region may not be reliable. The real-time fluoroscopy images obtained during the procedure were reviewed to ascertain this fact. Despite this fact, the apparent conductivity maps did indicate regions of slow conduction (detailed in Fig.12) near the septal region as can be seen from Fig.11c.

Once the apparent conductivity map/image of the particular endocardial surface has been estimated, we now proceed to demonstrate the efficacy of the fast electrophysiological model in its predictive capacity. Fig.13a shows the isochrones measured from the Ensite system for the same patient in a dual chamber pacing mode. The heart was paced endocardially in the apex of the left ventricle and in the right ventricle. The initialisation from the right ventricle reaches the left ventricular endocardium 20 ms after the initial depolarisation in response to left ventricular apical pacing. Fig.13b shows the isochrones estimated by the model using the apparent conductivity map (Fig.12) for this case. The left ventricular endocardial model was initialised (activated) with a value of 0 ms at the region indicated as Pacing Location 1 and another region indicated by Pacing Location 2 was initialised within 20 ms. By a visual comparison of Fig.13a and Fig.13b, it

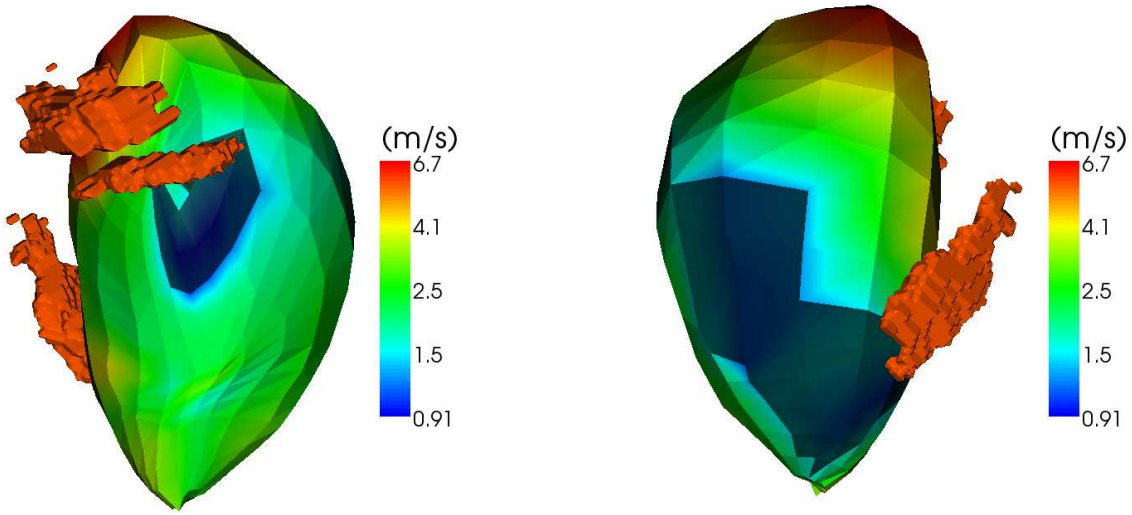

(a) (b)

Fig. 10. (a),(b) Estimated conduction velocity maps and comparison with scar locations. The black regions on the mesh are those regions identified with AC < 0.5 using the model and adaptive zonal estimation algorithm.

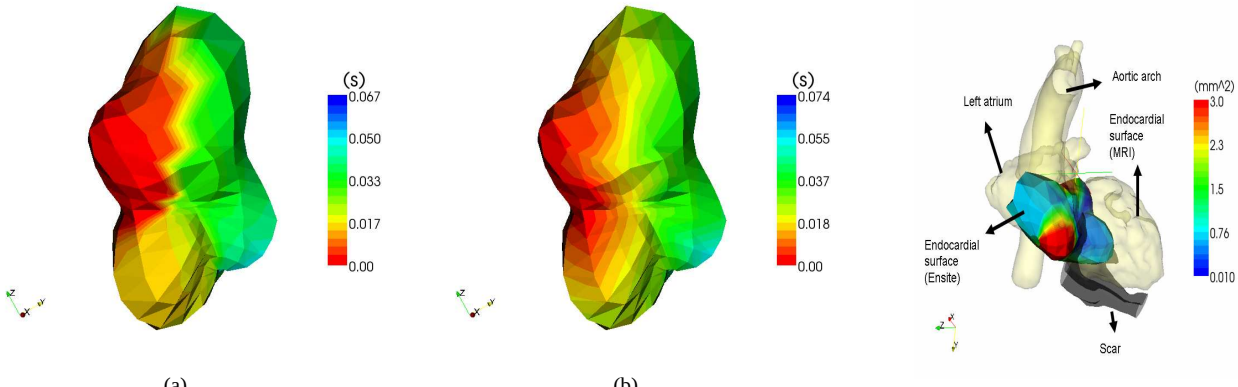

(a) (b) (c)

Fig. 11. (a),(b) Isochrones of depolarisation measured using Ensite and obtained after AC estimation (c) Ensite-MR-Scar registration.

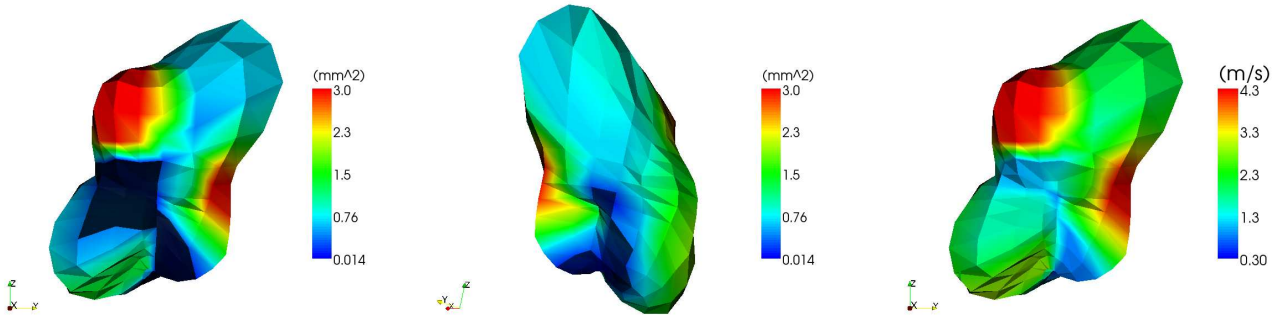

(a) (b) (c)

Fig. 12. (a),(b) Apparent conductivity images obtained after convergence of adaptive zonal estimation algorithm. The black regions indicate areas of low AC (c) Estimated conduction velocity.

can clearly be seen that the model with adjusted conductivity image is able to predict reasonable isochrones for a different pacing mode.

VI. Discussion

A. Parameter values and Mesh Resolution

The value of dimensionless constant $c_0 = 2.5$ in Equation (1) has been taken from literature [11]. As the ratio $c_0\sqrt{D}/\tau$ represents the velocity of the excitation front in the eikonal-diffusion equation and the typical propagation velocity values for normal myocardium reported using the Ensite system are about 2.0 m/sec [29], we chose a value of $\tau = 1.0$ ms obtained by using the value of λ_f for normal myocardial tissue as 0.8 mm. Further as we model the propagation only on the endocardial surface as compared to the ventricular volumetric tissue, we would expect the value of either c_0 or τ to be adjusted to represent higher propagation velocities. In this paper, we chose to take c_0 as the value specified in literature and modify the value of τ in order to increase the propagation velocity. For a given set of patient electrical activation times, varying c_0 or τ would change the magnitude of the apparent conductivity estimated but the identification of normal to diseased (low AC values) tissue would not be altered.

The anisotropic diffusion flow term is computed on a relatively coarse mesh. This is due to the following reasons

- As we only consider a surface, we do not have to precisely represent the transmural fibre variation, and as the fibre direction is quite smooth when considering only the endocardium, we do not need a very fine mesh.
- Further, such precise discretisation would be beneficial if we have the patient data at a similar resolution, which unfortunately is not the case with the present electro-anatomical mapping systems.
- Experiments done by increasing the mesh resolution for both synthetic and clinical data cases showed that the estimation algorithm obtains similar results as on the coarse mesh.

B. Fast electrophysiology model

The fast electrophysiology model presented in Section II is based on the eikonal-diffusion equation. The fast marching methodology applied to solve this nonlinear equation has considerable advantage in terms of obtaining the electrical wave pattern or the isochrones in order of seconds of computational time and hence can be potentially feasible to apply such a model in the clinical setting. A limitation of this model is that the solution methodology is only of first-order accuracy [14]. However, it can be seen that the 256 node meshes that we use in this study are able to obtain results with sufficient accuracy for the application that we consider (simulate LBBB pathology). Finally, the presented electrophysiology model needs to incorporate repolarisation effects of the tissue in order to model more complex electrical phenomena such as swirling waves which are encountered in other forms of cardiac arrhythmia. An initial development to simulate multi-front propagation was presented earlier in [15].

An important aspect of the anisotropic fast EP model presented in this paper is the cardiac fibre orientation. A generic formula of fibre directions (60^o to the circumferential direction on the mesh) was used in this paper and more accurate descriptions of the fibre directions and anisotropic ratio of space constants λ could be highly beneficial in modelling the electrical propagation more accurately.

C. Conduction parameter estimation

The adaptive zonal estimation algorithm based on simplified Brent's method (Section III) can be used in conjunction with the fast electrophysiology model to obtain additional conduction related parameter images. This algorithm has been shown to successfully estimate apparent conductivity values for both synthetic as well as clinical data. The global estimation algorithm eliminates the need for a very good initial guess of the AC value by the user and is shown to be quite robust. We obtain a very good initial guess from the global estimation algorithm in about 20 iterations. For the synthetic data experiment, the adaptive zonal AC estimation algorithm takes about another 20 iterations with about 5 refinement levels (i.e., about 32 zones) to obtain an acceptable map for AC. The time taken for the adaptive algorithm is about 10 min to reach up to 32 zones. The algorithm is also shown to be robust to fibre directions and hence can be used even if the fibre directions are not precisely known.

The minimisation method used in the algorithm relies on a few parameters, the initial bracketing and the convergence criterion defined for each level. A difference in the r.m.s error between two successive iterations lower than 0.01 is sufficient for the cases presented in this paper. An initial bracketing of the minimum is essential for the Brent's method to obtain convergence. The AC should always be positive and therefore we take a very small positive value for the lower bracket. Also, there is no particular maximum limit for the AC. We use an AC value of 10 as a realistic value of the upper limit for the bracketing at any Brent iteration in the adaptive algorithm.

D. Application to clinical data

We presented functional imaging of electrical conduction related parameter for two different left bundle branch block cases. The estimation algorithm requires less than an hour wall time to obtain an acceptable AC map (32 zones) for both clinical data sets. From the estimated AC functional images (Fig.9 and Fig.12), we can clearly identify regions of slower conduction (AC < 0.5). These slow conduction regions are also shown to be correlated with scar locations obtained from late enhancement images. Apparent conduction velocity maps can also be generated and we see that the velocity estimated lies in the range of 0.3 to 0.9 m/s in regions of scar to about 2.5 m/s for normal healthy tissue. A very high velocity in excess of 4 m/s is also observed in certain regions. This is probably due to the accuracy of the measured data from the Ensite system. We sometimes identify large regions of the endocardial surface being depolarised instantaneously - suggesting very high conduction velocities and the estimated conduction velocity maps reflect this behaviour present in the

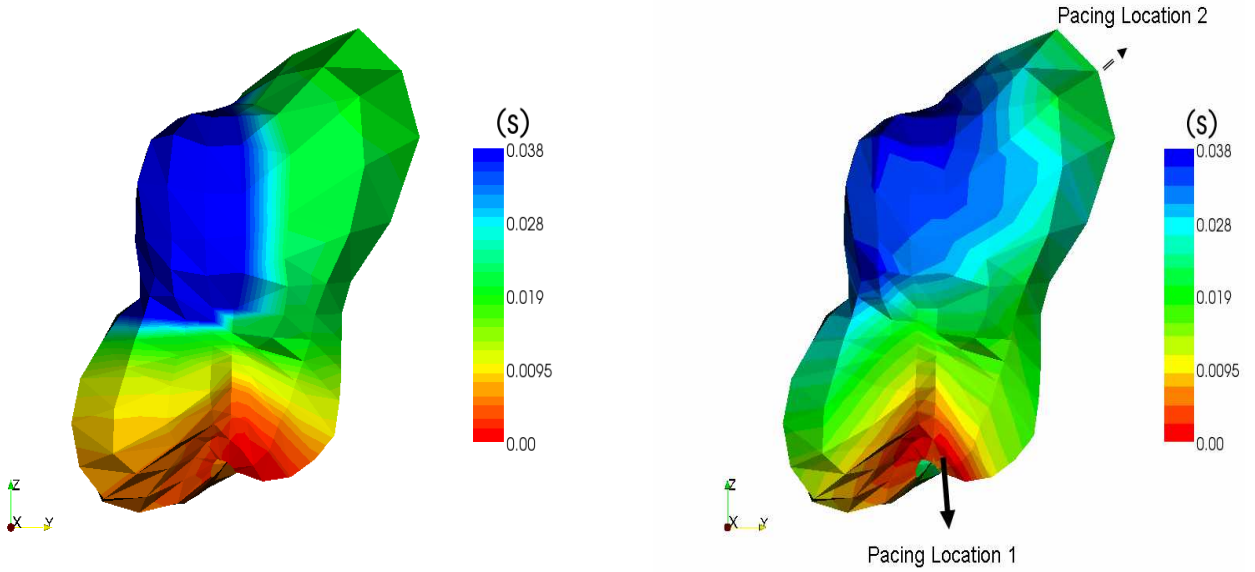

(a) Measured isochrones

(b) Predicted isochrones

Fig. 13. Usage of model in a predictive fashion: (a) Isochrones of depolarisation measured using Ensite in a dual chamber pacing mode (b) Isochrones of depolarisation predicted by the EP model with estimated sinus rhythm apparent conductivity map.

depolarisation time input. Furthermore as the estimated map is projected on a surface instead of the actual 3D ventricular volume, we expect the conduction velocities to be higher than the normally accepted values. The apparent conduction velocity values estimated in healthy regions from the presented adaptive zonal algorithm are consistent with values reported in studies using the Ensite system and estimated using Schilling's method [29].

Additionally, once the electrophysiological model is tuned to the particular patient parameters (once the AC has been estimated), we have shown that the tuned model is now able to simulate a different pacing protocol. We are now in the process of acquiring more clinical data in order to validate the presented methodology. Furthermore, the accuracy of such prediction capability could be highly improved by incorporating a 3D model which could simulate the propagation on the whole ventricular volume and this is a subject of ongoing work.

VII. Conclusions

We presented a new method of imaging electrical conduction parameter in the heart based on a fast electrophysiological model and an adaptive parameter estimation procedure. The presented EP model is based on the eikonal approach and can accurately simulate the propagation of the depolarisation wavefront on the endocardial surface. A novel adaptive zonal estimation for the conductivity parameter (apparent conductivity) has been proposed to tune the electrophysiological model to measured isochrones of depolarisation. The estimation algorithm has also been shown to be robust to the operator's initial estimate and to cardiac fibre orientations. The apparent conduction images obtained using this procedure have been validated on synthetic as well as clinical data. Possible regions of slow conduction have been identified and shown to correlate with scar locations obtained using late enhancement MR image segmentations using this procedure. Finally, we have presented a proof of concept for the electrophysiology model, tuned to an individual patient data, to be capable of simulating the electrical wave propagation for different pacing modes. Having such a model opens up possibilities for early detection of scarred regions responsible for arrhythmia, and could also aid in the planning of interventional procedures.

There can be several improvements made to the proposed model to enhance its estimation properties which will be the focus of our future research. Some of them are outlined here. In terms of simulation, higher order FMM algorithms can be incorporated to obtain better resolution of propagating wavefronts. The apparent conduction algorithm can be improved by incorporating gradient minimisation methods with a suitable adjoint formulation instead of Brent's optimisation at each level and better regularisation techniques. Finally, we also intend to introduce the time term into the eikonal-diffusion equation so as to simulate multi-front propagation incorporating both depolarisation and repolarisation phenomena and extension of these methods to volumetric meshes. Incorporation of a mechanical component into the model is also the subject of ongoing work, whereby we envisage an electro-mechanical model which could be used to simulate both different pathologies and treatment strategies. Preliminary work has been done towards the adjustment of mechanical models to clinical data, however there are still some challenging difficulties [30].

ACKNOWLEDGEMENTS

The authors would like to acknowledge Steven Sinclair, research radiographer at the Division of Imaging Sciences and Julian Bostock and cardiac technicians at Guy's and St.Thomas' NHS foundation trust for their support in acquisition of the clinical data utilised in this paper.

REFERENCES

[1] J. G. F. Cleland, J.-C. Daubert, E. Erdmann, N. Freemantle, D. Gras, L. Kappenberger, and L. Tavazzi, "The effect of cardiac resynchronization on morbidity and mortality in heart failure," *The New England Journal of Medicine*, vol. 352, no. 15, pp. 1539–1549, 2005.

[2] J. Sra and S. Ratnakumar, "Cardiac image registration of the left atrium and pulmonary veins," *Heart Rhythm*, vol. 5, no. 4, pp. 609–617, 2008.

[3] K. S. Rhode, M. Sermesant, D. Brogan, S. Hegde, J. Hipwell, P. Lambiase, E. Rosenthal, C. Bucknall, S. A. Qureshi, J. S. Gill, R. Razavi, and D. L. G. Hill, "A system for real-time XMR guided cardiovascular intervention," *IEEE Trans. on Med. Imaging*, vol. 24, no. 11, pp. 1428–1440, 2005.

[4] C. Luo and Y. Rudy, "A model of the ventricular cardiac action potential. depolarization, repolarization and their interaction," *Circ. Res.*, vol. 68, no. 6, pp. 1501–1526, 1991.

[5] C. H. Luo and Y. Rudy, "A dynamic model of the cardiac ventricular action potential. simulations of ionic currents and concentration changes," *Circ. Res.*, vol. 74, no. 6, pp. 1071–1097, 1994.

[6] R. FitzHugh, "Impulses and physiological states in theoretical models of nerve membrane," *Biophys. J.*, vol. 1, pp. 445–466, 1961.

[7] F. Fenton and A. Karma, "Vortex dynamics in three-dimensional continuous myocardium with fiber rotation-filament instability and fibrillation," *Chaos*, vol. 8, pp. 20–47, 1998.

[8] O. Bernus, R. Wilders, C. Zemlin, H. Verschelde, and A. Panfilov, "A computationally efficient electrophysiological model of human ventricle cells," *Am. J. Physiol. Heart, Circ. Physiol.*, vol. 282, no. 6, pp. 2296–2308, 2002.

[9] K. H. W. J. ten Tusscher, D. Noble, P. J. Noble, and A. V. Panfilov, "A model for human ventricular tissue," *Am. J. Physiol. Heart, Circ. Physiol.*, vol. 286, no. 4, pp. 1573–1589, 2003.

[10] J. P. Keener, "An eikonal-curvature equation for action potential propagation in myocardium," *J. Math. Biol.*, vol. 29, pp. 629–651, 1991.

[11] K. A. Tomlinson, P. J. Hunter, and A. J. Pullan, "A finite element method for an eikonal equation model of myocardial excitation wavefront propagation," *SIAM Journal of Applied Mathematics*, vol. 63, no. 1, pp. 324–350, 2002.

[12] J. Sethian, *Level Set Methods and Fast Marching Methods*. CUP, 1999.

[13] P. C. Franzone, L. Guerri, and S. Rovida, "Wavefront propagation in activation model of the anisotropic cardiac tissue," *J. Math. Biol.*, vol. 28, no. 2, pp. 121–176, 1990.

[14] M. Sermesant, Y. Coudiere, V. Moreau-Villéger, K. S. Rhode, D. L. G. Hill, and R. S. Razavi, "A fast marching approach to cardiac electrophysiology simulation for XMR interventional imaging," in *Medical Image Computing and Computer-Assisted Intervention*, J. Duncan and G. Gerig, Eds., 2005, pp. 607–615.

[15] M. Sermesant, E. Konukoglu, H. Delingette, Y. Coudiere, P. Chinchapatnam, K. S. Rhode, R. Razavi, and N. Ayache, "An anisotropic multi-front fast marching method for real-time simulation of cardiac electrophysiology," in *Functional Imaging and Modelling of the Heart*, 2007.

[16] P. Chinchapatnam, K. S. Rhode, A. P. King, G. Gao, Y. Ma, T. Schaeffter, D. J. Hawkes, R. Razavi, D. L. G. Hill, S. R. Arridge, and M. Sermesant, "Anisotropic wave propagation and apparent conductivity estimation in a fast electrophysiological model: Application to XMR interventional imaging," in *Medical Image Computing and Computer-Assisted Intervention (1)*, ser. Lecture Notes in Computer Science, N. Ayache, S. Ourselin, and A. Maeder, Eds., vol. 4791. Springer, 2007, pp. 575–583.

[17] R. J. Schilling, N. S. Peters, J. Goldberger, A. H. Kadish, and D. W. Davies, "Characterization of the anatomy and conduction velocities of the human right atrial flutter circuit determined by noncontact mapping," *J. Am. Coll. Cardiol.*, vol. 38, no. 2, pp. 385–393, 2001.

[18] L. W. Wang, H. Y. Zhang, and P. C. Shi, "Simultaneous recovery of three-dimensional myocardial conductivity and electrophysiological dynamics: a nonlinear system approach," *Computers in Cardiology*, vol. 33, pp. 45–48, 2006.

[19] V. Moreau-Villéger, H. Delingette, M. Sermesant, H. Ashikaga, E. McVeigh, and N. Ayache, "Building maps of local apparent conductivity of the epicardium with a 2-D electrophysiological model of the heart," *IEEE Trans. Biomed. Eng.*, vol. 53, no. 8, pp. 1457–1466, 2006.

[20] K. A. Tomlinson, "Finite elements solution of eikonal equation for excitation wavefront propagation in ventricular myocardium," Ph.D. dissertation, The University of Auckland, New Zealand, 2000.

[21] P. A. Friedman, "Novel mapping techniques for cardiac electrophysiology," *Heart*, vol. 87, pp. 575–582, 2002.

[22] L. Gepstein, G. Hayam, and S. A. Ben-Haim, "A novel method for nonfluoroscopic catheter-based electroanatomical mapping of the heart," *Circulation*, vol. 95, pp. 1611–1622, 1997.

[23] W. Press, B. Flannery, S. Teukolsky, and W. Vetterling, *Numerical Recipes in C*. Cambridge Univ. Press, 1991, ch. Minimization or maximization of functions, pp. 290–352.

[24] J.-M. Peyrat, M. Sermesant, X. Pennec, H. Delingette, C. Xu, E. R. McVeigh, and N. Ayache, "A computational framework for the statistical analysis of cardiac diffusion tensors: application to small database of canine hearts," *IEEE Trans. on Med. Imaging*, vol. 26, no. 11, pp. 1500–1514, 2007.

[25] R. J. Schilling, N. S. Peters, and D. W. Davies, "Simultaneous endocardial mapping in the human left ventricle using a noncontact catheter: Comparison of contact and reconstructed electrograms during sinus rhythm," *Circulation*, vol. 98, pp. 887–898, 1998.

[26] K. Rhode, D. Hill, P. Edwards, J. Hipwell, D. Rueckert, G. Sanchez-Ortiz, S. Hegde, V. Rahunathan, and R. Rezavi, "Registration and tracking to integrate x-ray and mr images in an xmr facility," *IEEE Trans. on Med. Imaging*, vol. 22, 2003.

[27] N. Toussaint, M. Sermesant, and P. Fillard, "vtkinria3d: A vtk extension for spatiotemporal data synchronization, visualization and management," in *Proc. of Workshop on Open Source and Open Data for MICCAI*, Brisbane, Australia, October 2007.

[28] M. Sermesant, K. Rhode, G. Sanchez-Ortiz, O. Camara, R. Andriantsimiavona, S. Hegde, D. Rueckert, P. Lambiase, C. Bucknall, E. Rosenthal, H. Delingette, D. Hill, N. Ayache, and R. Razavi, "Simulation of cardiac pathologies using an electromechanical biventricular model and XMR interventional imaging," *Medical Image Analysis*, vol. 9, no. 5, pp. 467–480, 2005.

[29] P. D. Lambiase, A. Rinaldi, J. Hauck, M. Mobb, D. Elliott, S. Mohammad, J. S. Gill, and C. A. Bucknall, "Non-contact left ventricular endocardial mapping in cardiac resynchronization therapy," *Heart*, vol. 90, pp. 44–51, 2004.

[30] M. Sermesant, P. Moireau, O. Camara, J. Sainte-Marie, R. Andriantsimiavona, R. Cimrman, D. L. Hill, D. Chapelle, and R. Razavi, "Cardiac function estimation from MRI using a heart model and data assimilation: Advances and difficulties," *Medical Image Analysis*, vol. 10, no. 4, pp. 642–656, 2006.